

ICNMM2018-7628

## EVAPORATION FROM A SIMULATED SOIL PORE: EFFECTS OF RELATIVE HUMIDITY

**Partha P. Chakraborty**  
Kansas State University  
Manhattan, Kansas, USA  
parthapratim@ksu.edu

**Melanie M. Derby**  
Kansas State University  
Manhattan, Kansas, USA  
derbym@ksu.edu

### ABSTRACT

Reduction of irrigation is a pressing issue in the food-water-energy nexus. Around two-third of global water withdrawals are used for irrigation in the areas with insufficient rainfall. In the U.S. Central High Plains, the Ogallala Aquifer is responsible for providing water for the production of corn, wheat, soybeans, and cattle; reducing the evaporation of water from soil provides an excellent opportunity to decrease the need for irrigation. In this paper, evaporation of sessile 4- $\mu$ l water droplets from a single simulated soil pore was observed. Soil pores were created using three 2.35-mm hydrophilic glass or hydrophobic Teflon beads of the same size. The experiments were conducted at the same temperature (20° C) and two relative humidity levels, 45% and 60% RH. Evaporation times were recorded and the transport phenomena were captured using a high-speed camera. Relative humidity directly affected evaporation; evaporation times were lower at the lower RH. The glass surface had higher wettability and therefore the droplets were more stretched on the glass beads, more droplet-air areas were created and evaporation times were approximately 30 minutes at 60% RH. The Teflon surface was hydrophobic, for which air-water contact areas were lower, and evaporation times were longer – approximately 40 minutes at 60% RH. As evaporation progressed, a liquid island formed between two beads at both 45% and 60% RH in for glass and Teflon pores. The rate of decrease of the radius of the liquid island was shorter in Teflon than glass beads, which corresponded to lower evaporation rates from Teflon.

**Keywords:** *Relative humidity, evaporation, wettability, hydrophobic, hydrophilic.*

### INTRODUCTION

Food, energy, and water systems are inherently connected; new innovations are required to feed the growing global population (e.g., UN estimate of 9.8 billion people by 2050 [1])

without a significant increase in arable land [2]. Worldwide, agriculture is responsible for two-thirds of water withdrawals in order to supplement rainfall with irrigation in many productive, agricultural areas [3]. In the United States, withdrawal rates of the Ogallala aquifer in the Central High Plains greatly exceed the natural replenishment rate [4, 5]. Understanding and reducing evaporation from soils by altering soil wettability is one approach to reduce irrigation demands. Previous research demonstrated that evaporation from hydrophobized soils can be up to 50-65% lower than hydrophilic soils [6-9]. Shokri et al. [9] studied evaporation from sand columns with air conditions of 25.9°C and 22% RH over 30 days. The largest evaporative mass loss was observed from the 25-mm-deep hydrophilic column and the lowest evaporative losses were observed in the 25-mm-deep hydrophobic column and 18-mm hydrophilic/7-mm hydrophobic column.

Researchers have studied evaporation of sessile water droplets from hydrophilic and hydrophobic surfaces. Concentration gradients (i.e., humidity) [10], droplet pinning/contact line dynamics [10-14], and droplet contact areas and contact angles [11, 14, 15] were shown to be important parameters governing the evaporative process. The review by Erbil [16] regarding sessile droplet evaporation noted that the phenomena are complex and most papers assumed quasi-static conditions. Evaporation is motivated by a concentration difference and, if the ideal gas law is applicable, the concentration equals the vapor pressure of liquid at the given temperature or the difference between saturation and relative humidity.

Several researchers analyzed evaporating water droplets using a diffusion approach (i.e., based on the evaporative flux from the vapor concentration gradient in the gas phase near the droplet) [10-12, 15]. Hu and Larson [10] experimentally, analytically, and numerically investigated evaporation of sessile, pinned water droplets. The droplets were modeled as spherical

caps and they used the LaPlace equation with a time-dependent droplet interface to model droplet profiles. Net evaporation rates were approximately constant for contact angles (CA) <40°. Overall, for hydrophilic surfaces (CA < 90°), the evaporation rate,  $\dot{m}(t)$ , was

$$\dot{m}(t) = -\pi r D (1 - RH) c_v (0.27\theta^2 + 1.3) \quad (1)$$

where  $r$  is droplet radius,  $D$  is water vapor diffusivity,  $RH$  is relative humidity in decimal form,  $c_v$  is saturated water concentration, and  $\theta$  is contact angle in radians. The difference in relative humidity between the saturated water droplet and air-water mixture is the driving potential for evaporation. In their experiments, droplets were pinned during evaporation for 90-95% of total evaporation time.

Nguyen et al. [11] also solved the LaPlace equation for an evaporating droplet with diffusion and real boundary conditions and compared their results to water evaporation from hydrophobized [i.e., OTS (advancing CA 110°) and octanol (advancing CA 58°)] silicon and a bulk Teflon surface (advancing CA 120°). Experiments were performed at 25 °C, 55% RH. The droplets were viewed from side using a tensiometer and the droplet profile was fit with a LaPlacian curve (Fick’s law). In the first stage of evaporation, droplets on hydrophilic surfaces were pinned; for the second stage, contact angle was constant and wetted area changed. Evaporation times were higher for droplets on hydrophobic surfaces than on hydrophilic surfaces.

Birdi and Vu [13] studied evaporation of water droplets on glass (CA 41°) and Teflon (CA 108°). For the hydrophilic case, evaporation was generally linear with respect to time and the drop was primarily pinned. For the hydrophobic case, evaporation was nonlinear and the hydrophobic contact angle was maintained while the droplet area in contact with the surface decreased. Similarly, Orejon et al. [14] studied air-fluid-solid contact lines during the evaporation of water on glass (CA 28°), silicon (CA 57°), Cytop (CA 108°) and Teflon (CA 114°), and other fluid-surface combinations. They observed differences in contact angle dynamics depending on the surface hydrophobicity. On hydrophilic surfaces, the contact line was pinned initially (e.g., 40% of water droplet lifetime on silicon), whereas on hydrophobic surfaces, there was a slight, initial decrease in contact angle and then the contact angle remained steady until the final evaporation stage. Fewer studies investigated non-spherical droplet evaporation; Saenz et al. [17] studied sessile 1–7  $\mu\text{L}$ , pinned, non-spherical droplets. They noted that evaporation was not merely a function of droplet-air interface, and was affected by droplet shape and curvature.

The research objectives of this paper are to study the effects of hydrophobicity on evaporation dynamics from a single (i.e., three bead) pore at two different humidity levels [45% and 60% relative humidity (RH)].

## EXPERIMENTAL METHODS

Evaporation of sessile deionized water droplets from simulated soil pores were observed. The droplet volume was kept constant (4- $\mu\text{L}$ ) using a 0.2-2.0  $\mu\text{L}$  pipette. Food coloring (i.e., 2-3% volume) was mixed with the deionized water in order to

improve contrast for imaging. Simulated soil pores were created with three beads of hydrophilic glass and hydrophobic Teflon [polytetrafluoroethylene (PTFE)] and the beads diameters were 2.35 mm and placed in an environmental chamber (Figure 1). The center-to-center bead spacing was approximately 3.15 mm as shown in Figure 2. A fixed structure was constructed using 3D printing and was used to hold the three beads in their position and the droplet of water was placed in the pore created by three beads (Figure 2).

Experiments were conducted in a closed, environmental chamber which maintained air pressure, relative humidity and temperature. In these experiments, pressure was atmospheric (101.3 kPa) and the temperature was 20°C for all replications. The experiments were conducted for 45% and 60% RH to observe its effects on evaporation for quiescent conditions. A fluorescent lamp with magnetic base was used to provide sufficient lighting. The evaporation phenomena were captured using a high-speed camera (Fastec Motion Controller) and the evaporation times were recorded. The captured files were processed later with Active Presenter and PFV software.

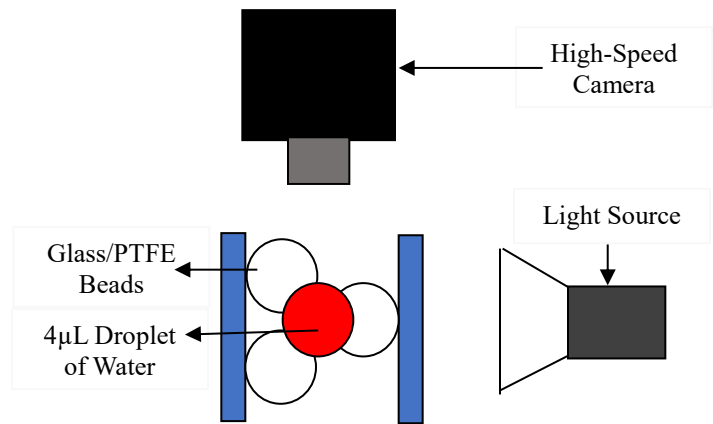


**Figure 1: Schematic of experimental apparatus located in an environmental chamber**

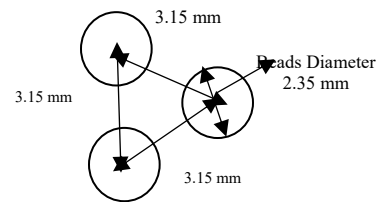


**Figure 2: Center-to-center bead spacing**

**Table 1: Experimental conditions**

Parameters	Numerical value
Relative humidity (RH)	30%, 45%, 60%, 75%
Pressure (kPa)	101.325
Temperature (°C)	20
Bead diameter (mm)	2.35
Volume of water droplet ( $\mu\text{L}$ )	4

## RESULTS AND DISCUSSION

Evaporation experiments were conducted at  $T=20\text{ }^{\circ}\text{C}$  and 45% and 60% RH for both hydrophilic glass and hydrophobic Teflon pores (Table 1). Each experimental condition was replicated four times. Figure 3 shows evaporation from the glass pore at 45% RH and Figure 4 shows evaporation from the glass bead at 60% RH. The overall average evaporation time was 26 minutes for 45% RH and 34 minutes for 60% RH (Table 2). As shown in equation (1), evaporation was directly dependent on relative humidity. For larger driving potential differences (i.e., lower air relative humidities), evaporation times were shorter.

The droplet was initially placed in the pore (Figures 3a and 4a) and decreased in size. Subsequently, the droplet depinned and formed forming one or two liquid islands between two droplets (Figure 3d-f and 4d-f). A liquid island was observed to form between two beads as shown in Figures 3(e) and 4(e). The liquid islands formed on the glass pore at approximately 14-15 minutes for 45% RH and 18-19 minutes at 60% RH. The approximate time of liquid island formation are presented in Table 3. Liquid depinning was not a major effect observed by Hu and Larson [10] and Nguyen et al. [11] for the evaporation of water from flat, hydrophilic surfaces. Depinning occurred in these experiments due to the rounded pore geometry. For evaporation from non-spherical droplet, Saenz et al. [17] noted that droplet shape affected evaporation.

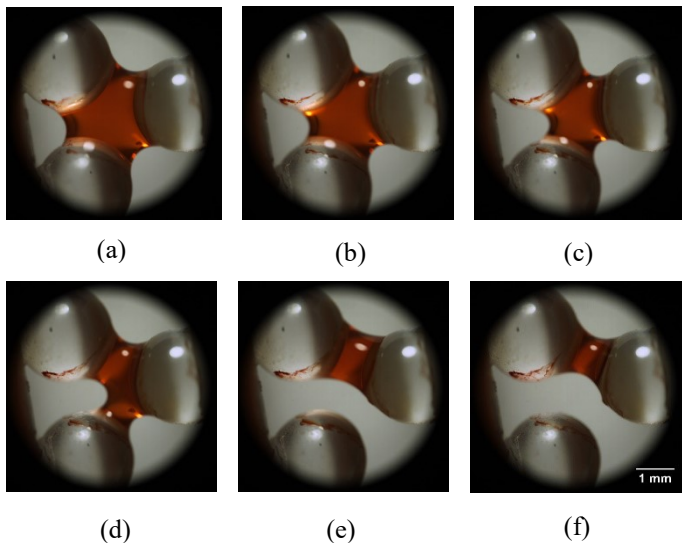


**Figure 3: Evaporation of water 4  $\mu\text{L}$  droplet at 45% RH from glass pore, (a) the initial position ( $t=0\text{ min}$ ); (b), (c), (d), (e) and (f) are evaporation phenomena at  $t= 6, 12, 14, 15$  and  $21$  minutes, respectively.**

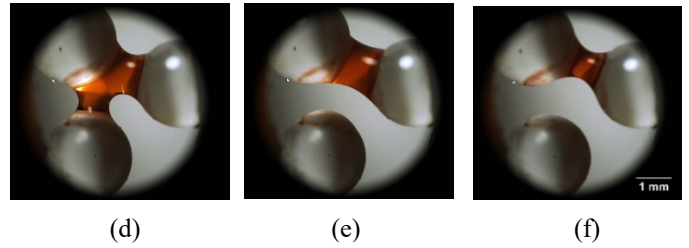
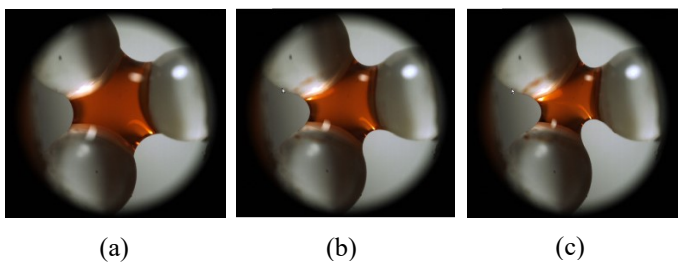


**Figure 4: Evaporation of water 4  $\mu\text{L}$  droplet at 60% RH from glass pore, (a) the initial position ( $t=0\text{ min}$ ); (b), (c), (d), (e) and (f) are evaporation phenomena at  $t= 9, 15, 17, 18$  and  $27$  minutes respectively.**

**Table 2: Evaporation time for 3 glass beads (45%/60% RH)**

45% RH		60% RH	
Replication Number	Evaporation Time (Minutes)	Replication Number	Evaporation Time (Minutes)
1	27	1	32
2	26	2	33
3	27	3	35
4	25	4	34
Average Time: <b>26 minutes</b>		Average Time: <b>34 minutes</b>	

**Table 3: Time of liquid island formation between two beads**

45% RH		60% RH	
Replication number	Time for liquid island formation (Minutes)	Replication number	Time for liquid island formation (Minutes)
1	15	1	18
2	16	2	19
3	10	3	21
4	12	4	18
Average Time: <b>13 minutes</b>		Average Time: <b>19 minutes</b>	

Similarly, experiments were conducted for a Teflon pore at 45% and 60% RH (Figures 5 and 6, respectively) and average evaporation times were 29 and 42 minutes, respectively. The average evaporation times were longer for the hydrophobic pore compared to the hydrophilic pore; this is likely impacted by the higher Teflon contact angle and therefore smaller droplet surface area [13]. Like the glass beads, a liquid island was observed to form between two Teflon beads. From Figure 5(e) and 6(e), it can be observed that the approximate times for liquid island are 17-18 minutes and 28-29 minutes at 45% and 60% RH, respectively. Liquid island formation times in the Teflon pore exceed those observed in the glass pore.

**Table 4: Evaporation time for 3 Teflon Beads (45%/60% RH)**

45% RH		60% RH	
Replication Number	Evaporation Time (Minutes)	Replication Number	Evaporation Time (Minutes)
1	32	1	38
2	28	2	44
3	29	3	43
4	29	4	41
Average Time: <b>29 minutes</b>		Average Time: <b>42 minutes</b>	

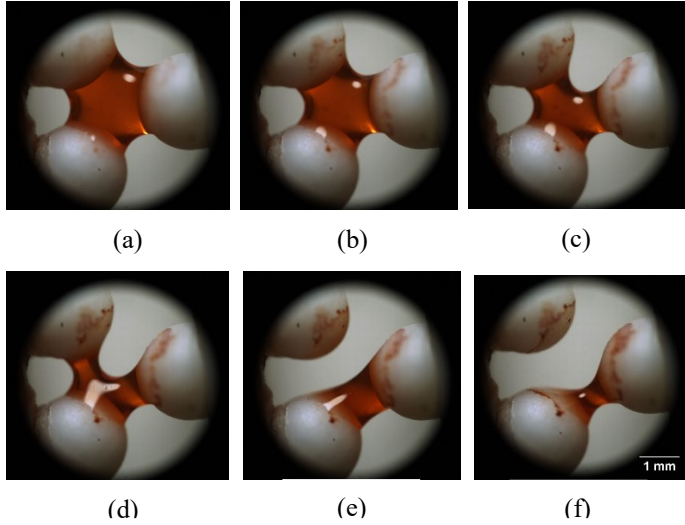


**Figure 5: Evaporation of water 4 µL droplet at 45% RH from Teflon pore; (a) the initial position ( $t=0$  min). (b), (c), (d), (e) and (f) are evaporation phenomena at  $t= 9, 12, 16, 17$  and  $24$  minutes respectively.**

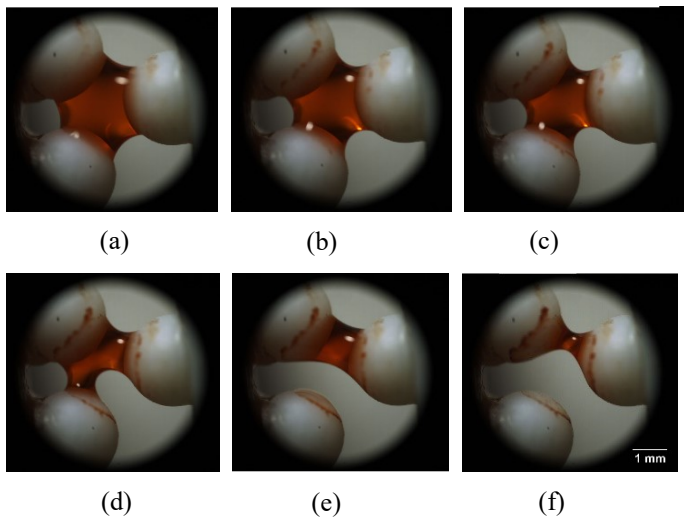


**Figure 6: Evaporation of water 4 µL droplet at 60% RH from Teflon pore; (a) the initial position ( $t=0$  min). (b), (c), (d), (e) and (f) are evaporation phenomena at  $t= 12, 18, 27, 28$  and  $42$  minutes respectively.**

**Table 5: Time of liquid island formation between two beads**

45% RH		60% RH	
Replication number	Time for liquid island formation (Minutes)	Replication number	Time for liquid island formation (Minutes)
1	21	1	28
2	17	2	28
3	19	3	28
4	15	4	29
Average Time: <b>18 minutes</b>		Average Time: <b>28 minutes</b>	

From the images presented in Figures 3–6, it is clear that evaporation depended on relative humidity. At 45% RH, the average evaporation time for glass and Teflon beads were 26 and 29 minutes, respectively. At 60% RH, the average evaporation times were 34 and 42 minutes, respectively. Evaporation corresponded to the difference in relative humidity, which can also be expressed using humidity ratio,  $\omega$ ,

$$\omega = \frac{m_v}{m_a} = 0.622 \frac{p_v}{p - p_v} \quad (2)$$

where  $m_v$  is the mass of water vapor,  $m_a$  is the mass of dry air,  $p_v$  is the partial pressure of water vapor, and  $p$  is total pressure. At  $T= 20^\circ\text{C}$ , psychrometrics yielded humidity ratios of 0.00652 kg/kg at 45% RH and 0.00873 kg/kg at 60% RH. For the liquid droplet, the humidity ratio is 0.0146 kg/kg, so driving potential for evaporation at 45% RH (i.e., 0.0081 kg/kg) is greater than the driving potential at 60% RH (i.e., 0.0059 kg/kg), which corresponds to faster evaporation in the drier conditions.

In their pioneering work on soil evaporation, Philip and de Vries [18, 19] analyzed transport through liquid islands under a temperature gradient. Vapor diffusion rates are often 1.5–5 times that predicted by Fick’s diffusion law [18-23] and are termed enhanced vapor diffusion. Philip and de Vries [19] and de Vries [18] suggested this enhancement was due to temperature gradients and condensation and evaporation across liquid islands rather than pure vapor diffusion (Figure 7). At a liquid island under a temperature gradient, the theory suggested that condensation occurs at interface A while evaporation occurs at interface B. Due to a temperature gradient and phase change across the liquid island, at one side the radius of the liquid island will increase due to evaporation (interface B) and on the other side it will decrease due to condensation (interface A). The experiments conducted in the present work were conducted in a quiescent environment without a temperature gradient. Therefore, both sides of the liquid island should experience evaporation equally and, therefore, the radius of the curvature should decrease with time. The following analysis of liquid island analyzed the evaporation dynamics as well as the comparison of evaporation rates between glass and Teflon beads (Figure 8).

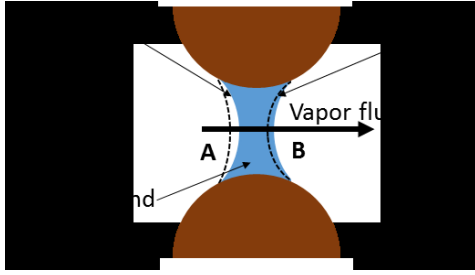


**Figure 7 Philip and de Vries model [18, 19] for enhanced vapor diffusion with condensation occurring at interface A and evaporation at interface B**

From Figure 8, it can be shown that the radius of the liquid island decreased with respect to time for glass and Teflon beads at 45% and 60% RH. The radius of the curvature was measured at 1-minute time intervals for both cases after the formation of a liquid island until the breakup of the liquid island, designated with an X in Figures 9 and 10. For evaporation from the glass beads, the liquid island radius decreased simultaneously and continuously after the formation of liquid island. In the case of Teflon beads, the liquid island was observed to form later than glass beads (Table-3 and Table-5) and it sustained its initial curvature before it decreased due to evaporation. In all cases, curvature appeared nearly symmetric; indicating evaporation from the liquid island based on the Philip and de Vries model [18, 19].

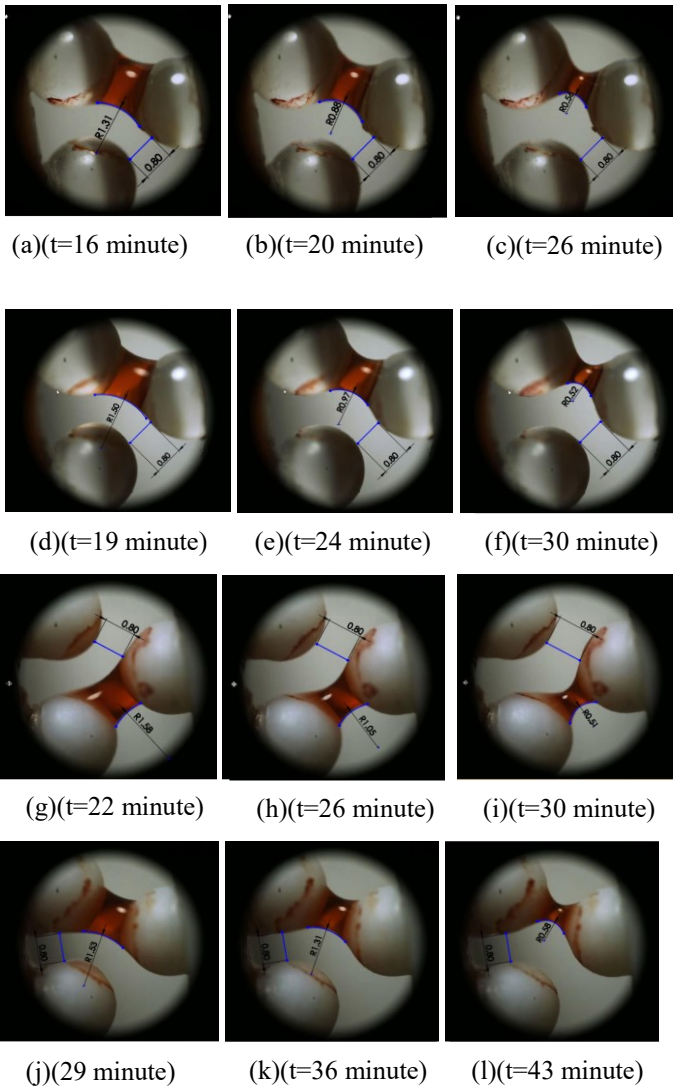


**Figure 8: Radius of the liquid island curvature; (a),(b),(c) and (d),(e),(f) show the radius of curvature of liquid island in glass beads at 45% and 60% RH respectively. (g), (h), (i) and (j), (k), (l) show the radius of the liquid island curvature in Teflon beads at 45% and 60% RH respectively.**

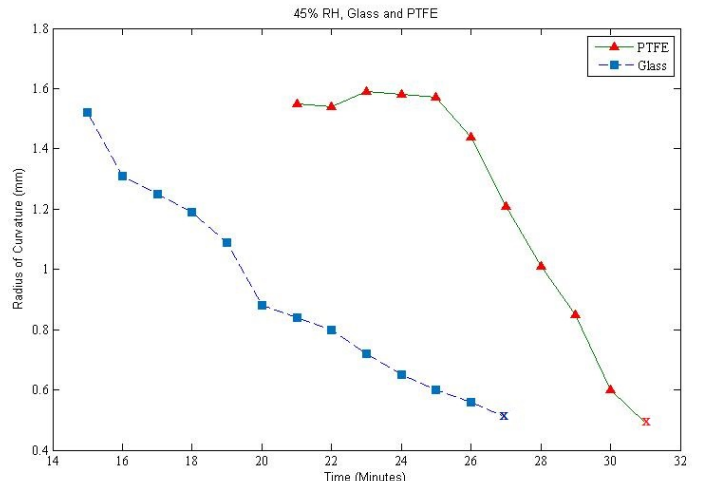


**Figure 9: Change of radius of the curvature of liquid island in glass and Teflon beads after liquid island formation at 45% RH. X represents breakup of the liquid island.**

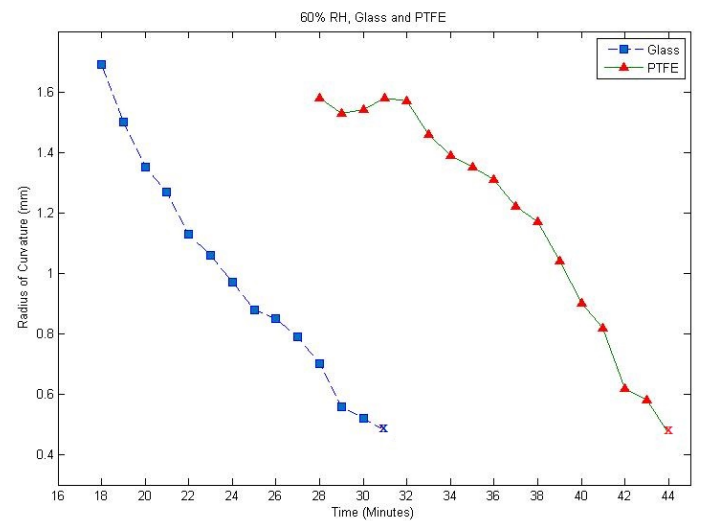


**Figure 10: Change of radius of the curvature of liquid island in glass and Teflon beads after liquid island formation at 60% RH. X represents breakup of the liquid island.**

The evolution of the liquid island radius was plotted for both glass and Teflon beads at 45% RH (Figure 9). The liquid island radius for evaporation from glass beads decreased more continuously than the Teflon one, whereas for evaporation from the Teflon beads, the liquid island sustained its initial radius for about 5 minutes and then decreased. In Figure 10, the change of liquid island radius for evaporation from glass and Teflon beads at 60% RH was plotted. Similar to evaporation at 45% RH, at 60% RH, the liquid island radius continually decreased for evaporation from the glass beads, while for the Teflon beads, the droplet sustained its initial radius for about 5 minutes before decreasing. The rate of evaporation depended on the decrease of the liquid island radius in course of time and was affected by surface wettability. In both cases (45% and 60% RH), after the formation of liquid island between two beads, the rate of change of radius of the liquid island was lower in the Teflon beads than glass. In glass beads, the radius decreased at a continuous rate from the beginning, i.e. the rate of evaporation was higher from the glass beads. Increasing rate of evaporation, also depicts that the droplet was more stretched in glass beads and thus the surface area was higher since glass is hydrophilic. During evaporation from the Teflon beads, the liquid island formed after it did on the glass beads due to the slower evaporation rates. From Figure 9 and Figure 10, the rate of decrease of the liquid island radius was lower for Teflon than glass, corresponding to a lower evaporation rate and therefore longer total evaporation time.

## CONCLUSIONS

Evaporation was observed from simulated soil pores comprised of hydrophilic glass and hydrophobic Teflon 2.35-mm-diameter beads. The following conclusions can be drawn:

- Evaporation times were longer at 60% RH compared to 45% RH for both hydrophilic and hydrophobic pores due to the driving potential (i.e., humidity) difference.
- Similarly, average evaporation times were longer for the hydrophobic, Teflon pore compared to the hydrophilic, glass pore.
- Liquid depinning occurred for droplets on both the hydrophilic and hydrophobic pores. The single droplet formed one or two liquid islands during evaporation.
- After the formation of a liquid island, the rate of change of the liquid island radius was lower for evaporation from Teflon beads than glass, (i.e. wettability affected liquid island dynamics and therefore evaporation times).

Future work is required to understand single-pore evaporation at additional relative humidities and pore geometries. Additional research is required to translate the fundamental knowledge of evaporation mechanisms into successful agricultural strategies to reduce evaporation.

## ACKNOWLEDGMENTS

The authors gratefully acknowledge the support of NSF CAREER grant number 1651451 and the Institute of Environmental Research

(IER) at KSU and Dr. Steve Eckels for the use of the environmental chambers.

## REFERENCES

- [1] 2017, "World population projected to reach 9.8 billion in 2050, and 11.2 billion in 2100," <https://www.un.org/development/desa/en/news/population/world-population-prospects-2017.html>.
- [1] 2017, "World population projected to reach 9.8 billion in 2050, and 11.2 billion in 2100," <https://www.un.org/development/desa/en/news/population/world-population-prospects-2017.html>.
- [2] Alexandratos, N., and Bruinsma, J., 2012, "World agriculture towards 2030/2050: the 2012 revision," ESA Working paper Rome, FAO.
- [3] Oki, T., and Kanae, S., 2006, "Global hydrological cycles and world water resources," *Science*, 313(5790), pp. 1068-1072.
- [4] Steward, D. R., and Allen, A. J., 2016, "Peak groundwater depletion in the High Plains Aquifer, projections from 1930 to 2110," *Agricultural Water Management*, 170, pp. 36-48.
- [5] Steward, D. R., Bruss, P. J., Yang, X., Staggenborg, S. A., Welch, S. M., and Apley, M. D., 2013, "Tapping unsustainable groundwater stores for agricultural production in the High Plains Aquifer of Kansas, projections to 2110," *Proceedings of the National Academy of Sciences*, 110(37), pp. E3477-E3486.
- [6] Bachmann, J., Horton, R., and Van der Ploeg, R., 2001, "Isothermal and nonisothermal evaporation from four sandy soils of different water repellency," *Soil Science Society of America Journal*, 65(6), pp. 1599-1607.
- [7] Davis, D. D., Horton, R., Heitman, J. L., and Ren, T., 2014, "An experimental study of coupled heat and water transfer in wettable and artificially hydrophobized soils," *Soil Science Society of America Journal*, 78(1), pp. 125-132.
- [8] Davis, D. D., Horton, R., Heitman, J. L., and Ren, T., 2009, "Wettability and hysteresis effects on water sorption in relatively dry soil," *Soil Science Society of America Journal*, 73(6), pp. 1947-1951.
- [9] Shokri, N., Lehmann, P., and Or, D., 2008, "Effects of hydrophobic layers on evaporation from porous media," *Geophysical Research Letters*, 35(19), p. L19407.
- [10] Hu, H., and Larson, R. G., 2002, "Evaporation of a sessile droplet on a substrate," *The Journal of Physical Chemistry B*, 106(6), pp. 1334-1344.
- [11] Nguyen, T. A., Nguyen, A. V., Hampton, M. A., Xu, Z. P., Huang, L., and Rudolph, V., 2012, "Theoretical and experimental analysis of droplet evaporation on solid surfaces," *Chemical engineering science*, 69(1), pp. 522-529.
- [12] Deegan, R. D., Bakajin, O., Dupont, T. F., Huber, G., Nagel, S. R., and Witten, T. A., 2000, "Contact line deposits in an evaporating drop," *Physical Review E*, 62(1), p. 756.
- [13] Birdi, K., and Vu, D., 1993, "Wettability and the evaporation rates of fluids from solid surfaces," *Journal of Adhesion Science and Technology*, 7(6), pp. 485-493.
- [14] Orejon, D., Sefiane, K., and Shanahan, M. E., 2011, "Stick-slip of evaporating droplets: substrate hydrophobicity and

- nanoparticle concentration," *Langmuir*, 27(21), pp. 12834-12843.
- [15] Birdi, K., Vu, D., and Winter, A., 1989, "A study of the evaporation rates of small water drops placed on a solid surface," *The Journal of Physical Chemistry*, 93(9), pp. 3702-3703.
- [16] Erbil, H. Y., 2012, "Evaporation of pure liquid sessile and spherical suspended drops: A review," *Advances in Colloid and Interface Science*, 170(1), pp. 67-86.
- [17] Sáenz, P., Wray, A., Che, Z., Matar, O., Valluri, P., Kim, J., and Sefiane, K., 2017, "Dynamics and universal scaling law in geometrically-controlled sessile drop evaporation," *Nature communications*, 8, p. 14783.
- [18] De Vries, D., 1958, "Simultaneous transfer of heat and moisture in porous media," *Eos, Transactions American Geophysical Union*, 39(5), pp. 909-916.
- [19] Philip, J., and De Vries, D., 1957, "Moisture movement in porous materials under temperature gradients," *Eos, Transactions American Geophysical Union*, 38(2), pp. 222-232.
- [20] Hillel, D., 1998, *Environmental soil physics*, Academic Press, San Diego, CA.
- [21] Jury, W., and Letey, J., 1979, "Water vapor movement in soil: reconciliation of theory and experiment," *Soil Science Society of America Journal*, 43(5), pp. 823-827.
- [22] Cary, J., 1963, "Onsage's relation and the non-isothermal diffusion of water vapor," *The Journal of Physical Chemistry*, 67(1), pp. 126-129.
- [23] Lu, S., Ren, T., Yu, Z., and Horton, R., 2011, "A method to estimate the water vapour enhancement factor in soil," *European Journal of Soil Science*, 62(4), pp. 498-504.